Title: Direct binding of a fungal effector by the wheat RWT4 tandem kinase activates defense

Authors:

Yi-Chang Sung[1], Yinghui Li[1, 2, 3], Suji Baik[1], Soichiro Asuke[4], Tzion Fahima[2], Gitta Coaker[1*]

Author Affiliations:

[1]Department of Plant Pathology, University of California, Davis, CA, U.S.A.

[2]Institute of Evolution and the Department of Evolutionary and Environmental Biology, University of Haifa, 199 Abba-Hushi Avenue, Mt. Carmel, 3498838 Haifa, Israel

[3]Triticeae Research Institute, Sichuan Agricultural University, Chengdu 611130, Sichuan, China

[4]Graduate School of Agricultural Science, Kobe University, Kobe 657-8501, Japan

* Corresponding author: G. Coaker, glcoaker@ucdavis.edu

Abstract:

Plants have intricate innate immune receptors that detect pathogens. Research has intensely focused on two receptor classes recognizing external and internal threats. Recent research has identified a new class of disease resistance proteins called tandem kinase proteins (TKPs). We investigated RWT4, a wheat TKP that confers resistance to the devastating fungal pathogen *Magnaporthe oryzae*. We established a rice protoplast system, revealing RWT4 specifically recognizes the AvrPWT4 effector, leading to the transcription of defense genes and inducing cell death. RWT4 possesses both kinase and pseudokinase domains, with its kinase activity essential for defense. RWT4 directly interacts with and transphosphorylates AvrPWT4. Biolayer interferometry revealed both RWT4 domains bind the effector. AlphaFold multimer modeling identified critical regions of RWT4 for effector interaction and recognition. These findings demonstrate that TKPs can directly bind a recognized effector and may act as primary immune receptors, circumventing traditional immune pathways.

Introduction

Plant genomes encode multiple innate immune receptors capable of recognizing diverse pathogen classes [1]. These immune receptors recognize pathogen features such as conserved molecular patterns or specialized secreted pathogen effector proteins [1]. The main classes of plant immune receptors are broadly categorized into cell-surface localized receptors, including receptor-like kinases (RLKs) or receptor-like proteins (RLPs), as well as intracellular nucleotide-binding domain leucine-rich repeat (NLR) immune receptors [2,3]. Most identified and well-studied receptors belong to RLKs/RLPs or NLRs, also known as canonical resistance genes [4]. Recently, kinase fusion proteins (KFP) have emerged as new players in plant immunity. KFPs contain unique protein architecture, including dual-kinase domains termed tandem kinase proteins (TKPs) or kinase fused with an integrated domain [5].

To date, more than 100 TKPs have been found across plant species, spanning both dicots and monocots [6,7]. TKPs represent a protein, not a gene, family since their kinase domains can be derived from different kinase (sub)families [8]. However, TKPs conferring disease resistance have been exclusively identified from the *Triticeae* tribe. Currently, ten *Triticeae* TKPs have been identified that confer resistance to biotrophic or hemibiotrophic fungal pathogens [5,8,9]. Barley RPG1 conferring resistance to barley stem rust was the first TKP identified [10]. Subsequent cloning of wheat resistance proteins, WTK1 to WTK7-TM and RWT4, also revealed dual-kinase architecture [6,9,11-13]. KFPs can also contain integrated non-kinase domains. For example, Sr43 (kinase-DUF347-DUF668) and WTK6-vWA (TKP-vWA), have been cloned with resistance to stem rust and leaf rust, respectively [14,15]. NLR immune receptors can also carry integrated domains responsible for directly binding recognized pathogen effectors, leading to defense activation and cell death [16]. However, it is unclear if TKPs can directly recognize pathogen effectors or other pathogen components.

Current data, primarily from mutant analyses, indicates that both domains are required for TKP-mediated resistance, which includes eliciting plant cell death. Wheat Tandem Kinase 1 (WTK1), conferring resistance to yellow rust, induces rapid and localized cell death post-haustoria

60 formation, suggesting that defense activation requires the perception of an unknown effector [8].
61 Mutagenesis assays have revealed the requirement of both kinase and pseudokinase domains for
62 WTK1 function [8]. Similarly, mutants in RPG1's kinase or pseudokinase domain exhibited full
63 susceptibility to *Puccina graminis f.* sp. *tritici* [17]. RPG1 exhibits *in vitro* autophosphorylation
64 activity, is rapidly phosphorylated upon exposure to avirulent spores, and can also induce cell
65 death [17,18]. These data indicate that TKPs are rapidly activated upon pathogen perception and can
66 elicit hallmarks of innate immune responses, including cell death [6,9,13,19,20].
67
68 Recently, the *Rwt4* TKP was cloned from the D-genome of hexaploid wheat [21]. RWT4 recognizes
69 the PWT4 effector from *Magnaporthe oryzae* (syn *Pyricularia oryzae*) pathotype *Avena*, leading
70 to an incompatible interaction [22]. *M. oryzae* is composed of host-specific subgroups that can cause
71 disease in rice, finger millet, oat, perennial ryegrass, and wheat. *M. oryzae* poses a threat to global
72 wheat production [23]. The *M. oryzae* host jump to wheat required loss of pathogen recognition by
73 the TKP *Rwt4* and the NLR *Rwt3* [21].
74
75 Here, we examined RWT4 as a model for TKP activation. We demonstrate that RWT4 directly
76 binds and phosphorylates the recognized effector AvrPWT4, but not an unrecognized VirPWT4
77 allele. Furthermore, RWT4 can be transferred to a rice protoplast system and confer defense
78 activation in the presence of AvrPWT4. Structure-function analyses identified key RWT4 residues
79 required for effector binding and defense activation. These findings provide detailed mechanistic
80 insights into TKP effector binding and activation.
81
82
83 **Materials and Methods**
84 ***Wheat infection assays***
85 Wheat seeds were pre-germinated on moistened filter papers. After 24 hours, sprouted seeds
86 were sown in the soil in seedling cases (5.5 × 15 × 10 cm, Sakata Prime Mix, Sakata Seed
87 Corporation, Yokohama, Japan), and grown at 22°C in a controlled-environment room with a 12-
88 h photoperiod of fluorescent lighting for eight days. Primary leaves of the nine-day-old seedlings

89 were fixed onto a hard plastic board with rubber bands just before inoculation. Conidial
90 suspensions (1×10^5 conidia/mL) were prepared as described previously [24] and sprayed onto fixed
91 primary leaves using an air compressor. The inoculated seedlings were incubated in a tray sealed
92 with plastic wrap under dark and humid conditions at 22°C for 24 h, then transferred to dry
93 conditions with a 12-h photoperiod of fluorescent lighting and incubated at 22°C for an additional
94 3-5 days. Four to six days after inoculation, symptoms were evaluated based on the size and color
95 of lesions [25]. The size of lesions was rated on six progressive grades from 0-5: 0 = no visible
96 infection; 1 = pinhead spots; 2 = small lesions (<1.5 mm); 3 = scattered lesions of intermediate
97 size (<3 mm); 4 = large typical lesion; and 5 = complete blighting of leaf blades. A disease score
98 comprised a number denoting the lesion size and a letter indicating the lesion color: 'B' for brown
99 lesions and 'G' for green lesions. The infection types 0, 1B, and 2B were regarded as resistant,
100 while the infection types 3G, 4G, and 5G were considered susceptible (Table S1).
101
102 ***Cloning and site-directed mutagenesis***
103 The *Rwt4* Cadenza allele (*Rwt4*^{Ca}, TraesCAD_scaffold_040753_01G000200.1) and Chinese Spring
104 allele (*Rwt4*^{Cs}, TraesCS1D02G058900) were codon-optimized for expression in rice and
105 synthesized (Twist Bioscience gene fragment). *Rwt4*$^{Ca_K217R/K327R}$ was generated by PCR-based site-
106 directed mutagenesis. Genes of interest were cloned to Gateway™ pENTR™ 4 Dual Selection
107 Vector (A10465) by NEBuilder HiFi DNA Assembly Master Mix (NEB, E2621L) and cloned to a
108 pUC19 expression vector powered by the maize ubiquitin promoter (*Zm*UBI) via Gateway LR
109 reaction. Full length of *Rwt4*^{Ca}, its kinase domain, and pseudokinase domain were cloned into *E.*
110 *coli* expression plasmids pET28a-His-MBP [26] or pET28a-His (EMD Biosciences) using ligation-
111 independent cloning (LIC) for recombinant protein production [27].
112
113 We refer to the *Pwt4* effector in two terms, the avirulent allele that can be recognized by *Rwt4*
114 (*AvrPwt4*) and a virulent form that cannot be recognized (*VirPwt4*) [22]. *AvrPwt4* (*Pwt4-Br58* type
115 allele, GeneBank:LC202655.1) and *VirPwt4* (*Pwt4-Br48* type allele, GenBank: LC202656.1), lacking
116 their N-terminal signal peptide as predicted by SignalP 5.0
117 (https://services.healthtech.dtu.dk/services/SignalP-5.0/), were codon optimized, synthesized

118 (Twist Bioscience gene fragment) and cloned into the pUC19:*Zm*UBI expression vector via
119 Gateway LR reaction. *AvrPwt4* and *VirPwt4* were cloned into an *E. coli* expression plasmid pET28a-
120 GST using ligation-independent cloning (LIC) for recombinant protein purification [27,28]. Sequences
121 were validated by whole plasmid sequencing service (Plasmidsaurus). All constructs and primers
122 used in this study are listed in Table S5 and Table S6.
123
124 ***Recombinant protein expression and purification***
125 Full length RWT4^{Ca}, the kinase domain, and the pseudokinase domain were expressed in *E. coli*
126 BL21 Rosetta (DE3) strain and purified by affinity and size exclusion chromatography. Four liters
127 of cells were grown at 37°C to OD_{600} of 0.4 before adding IPTG to a final concentration of 0.5 mM.
128 Cells were resuspended in a lysis buffer consisting of 50 mM Hepes pH 8.5, 300 mM NaCl, 1 mM
129 PMSF (phenylmethylsul-fonyl fluoride) and 1 µg/mL DNase and lysed by a microfluidizer at 18k
130 psi. The lysate was then clarified by centrifugation at 16000 g at 4°C for 50 min. The proteins of
131 interest were separated from the clarified lysate by immobilized metal affinity chromatography
132 (IMAC) and eluted with an elution buffer (50 mM HEPES at pH 8.5, 300 mM NaCl and 250 mM
133 imidazole) on an AKTA FPLC. Eluted samples were dialyzed into a low-salt buffer (20 mM Tris-HCl,
134 pH 8.5, 200 mM NaCl) for further affinity-based purification using 1 mL MBPTrapHP columns
135 (Cytiva Life Science, #29048641). Target proteins were eluted by a buffer (10 mM maltose, 20 mM
136 Tris-HCl, pH 8.5, 200 mM NaCl) and were injected to a HiLoad 16/600 Superdex 200 PG column
137 equilibrated with 10 mM HEPES at pH 8.0 and 150 mM NaCl. Fractions corresponding to the
138 proteins of interest were collected and visualized by Coomassie-stained SDS-PAGE, before being
139 concentrated using a 3 kDa MWCO Amicon Ultra centrifugal filter (Millipore Sigma, #UFC9003) to
140 appropriate concentrations for further analysis.
141
142 AvrPWT4 and VirPWT4 were expressed in *E. coli* BL21 Rosetta (DE3) and purified by affinity and
143 size exclusion chromatography. Their expression and cell lysates were prepared as described
144 above. Cell lysates were purified by affinity-based chromatography using 1mL GSTrap HP columns
145 (Cytiva Life Science, #17528201) equilibrated with a binding buffer 140 mM NaCl, 2.7 mM KCl, 10
146 mM Na_2HPO_4, 1.8 mM KH_2PO_4, pH 8.0. Target proteins were eluted with elution buffer (50 mM

147 Tris-HCl, 10 mM reduced glutathione, pH 8.0) and dialyzed to a buffer condition (10 mM Tris-HCl
148 pH 8.0, 150 mM NaCl, 0.5 mM EDTA, 1 mM DTT) optimized for TEV protease cleavage (ProTEV
149 Plus, Promega, V6101). Samples were adjusted to a final volume of 10 mL with 100U TEV protease
150 and incubated at 4°C for overnight. After the incubation, samples were loaded into a GSTrap HP
151 column (Cytiva Life Science, #17528201), and the flow-through was collected for further size
152 exclusion chromatography (HiLoad 16/600 Superdex 200 PG column) as described above. Purified
153 proteins were visualized by Coomassie-stained SDS-PAGE and concentrated using a 3 kDa MWCO
154 Amicon Ultra centrifugal filter (Millipore Sigma, #UFC9003,).
155
156 ***Kinase activity and phosphatase assays***
157 Kinase reactions were performed according to [29] with minor modifications. Kinase reactions were
158 performed in a kinase buffer consisting of 20 mM Tris-HCl (pH 7.5), 10 mM $MgCl_2$, 1 mM $CaCl_2$, 1
159 mM dithiothreitol, 100 µM ATP, with additional 10 µCi of [^{32}P]γATP (Revvity, #BLU002A100UC).
160 Two µg of recombinant protein was mixed with the mentioned buffer and reactions were
161 incubated at 30°C for 30 min and stopped with 3x Laemmli sample buffer. Radioactive samples
162 were separated on SDS-PAGE gels and visualized by autoradiography. For trans-phosphorylation
163 assays, RWT4^{Ca} and PWT4 were mixed at 1:1 ratio and incubated on ice for 20 min before the
164 mentioned kinase reaction. For phosphatase treatments, 2µg of recombinant protein was mixed
165 with 400U lambda protein phosphatase (NEB, #P0753S) at 30°C for 30 min before separated by
166 an SDS-PAGE. The phosphorylation status of RWT4 was visualized by a Western blot using an
167 Phospho-Threonine/Tyrosine Antibody (Cell signaling technology, #9381) at 1:2000 dilution in a
168 TBST buffer for an overnight incubation at 4°C. The antibody was detected by an Immun-Star Goat
169 Anti-Rabbit (GAR)-HRP Conjugate (Bio-Rad #1705046) and protein signals were detected on the
170 immunoblot using SuperSignal™ West Pico PLUS Chemiluminescent Substrate (ThermoFisher
171 Scientific #34580) and visualized by ChemiDoc™ Touch Gel Imaging System (Bio-Rad #1708370).
172
173 ***Mass spectrometry (MS)***
174 Kinase reactions using 6 ug of RWT4^{Ca} and AvrPWT4 were conducted as described above. Samples
175 were treated with freshly prepared 10mM dithiothreitol and 55 mM Iodoacetamide for reduction

176 and alkylation. Samples were digested by using trypsin at 10 ng/µL at 37°C overnight and peptides
177 were harvested by with 50% ACN/0.1% FA (formic acid, Sigma #06473), lyophilized and
178 resuspended with 0.1% FA. Samples were submitted to the Genomics Center Proteomics Core at
179 the University of California, Davis. Reverse-phased Liquid Chromatography (LC) was performed
180 on an EASY-nLC II HPLC (Thermofisher Scientific). The digested peptides were desalted by ZipTip
181 with 0.6 µL C18 resin (ZTC18S096, Millipore) before separated by a 75-µm × 150-mm C18 100A 3-
182 units reverse phased column at a flow rate 300 nL/min. The gradient elution employed buffer A
183 (0.1% formic acid) and buffer B (100% acetonitrile) over 60 min, transitioning from 5% to 35%
184 buffer B over 45 min, followed by a 35% to 80% buffer B gradient over 5 min, holding at 80%
185 buffer B for 2 min, and finally returning to 5% buffer B over 2min, maintaining at 5% buffer B for
186 6 min before the next sample injection.
187
188 Mass spectra were collected on an Orbitrap Exploris Mass Spectrometer (ThermoFisher Scientifics)
189 with one full scan (300–1,600 m/z, R = 60,000 at 200 m/z) at a target of 3x 10^6 ions, followed by
190 data-independent MS/MS scans with higher-energy collisional dissociation (HCD) detected in the
191 Orbitrap (R = 15,000 at 200 m/z). Results were analyzed by using the DIA-NN software package [30].
192 The phosphorylated peptides were mapped to the sequence of $RWT4^{Ca}$ and AvrPWT4. Peptide
193 spectra were visualized by using Skyline software package [31].
194
195 ***Bio-Layer Interferometry (BLI)***
196 BLI experiments were conducted by using the ForteBio Octet® RED384 equipment at the UC Davis
197 Octet® Real-Time Drug and Protein Binding Kinetics Unit. Analyte proteins (His-$RWT4^{Ca}$, MBP-His-
198 $RWT4^{Ca}$, MBP-His-KD and MBP-His-PKD) were diluted to 100nM in Octet® Kinetics Buffer
199 (SARTORIUS, #18-1105) for immobilized to Octet® Ni-NTA (NTA) Biosensors (SARTORIUS, #18-
200 5101). Ligand proteins (AvrPWT4 and VirPWT4, without tags, or GST) were prepared at 10 µM in
201 Octet® Kinetics Buffer as a stock solution for a 1.5x serial dilution to generate concentration
202 gradient. Wavelength measurement for the interaction between ligand and analyte proteins
203 followed the manufacturer's protocol with 600 sec for association and 600 sec for dissociation [32].
204

205 ***Yeast-two hybrid (Y2H)***

206 To validate RWT4 and PWT4 interactions, *Rwt4*^{Ca} and its variant proteins were cloned into the
207 prey vector pGADT7 (Takara, #630442) while *AvrPwt4* and *VirPwt4* were cloned into the bait
208 vector pGBKT7 (Takara, #630443). These constructs were co-transformed into the yeast strain
209 AH109 following the manufacturer's instructions from Frozen-EZ Yeast Transformation II™ (Zymo
210 Research). Yeast transformation was tested by dilution plating cells from a starting concentration
211 of OD_{600} 5.0 on double drop out (DDO) plates (SD-2: SD/-Trp/-Leu), while interactions were
212 confirmed through quadruple drop out (QDO) selection (SD-4: SD/-Trp/-Leu/-His/-Ade/3-AT). 3-
213 AT (3-amino-1,2,4-triazole) was used at 10 mM to reduce background HIS activation. The
214 transformed yeast cells were incubated at 30°C for two to five days before imaging.

215

216 For protein expression in yeast cells, five mL of yeast cells containing the genes of interest were
217 grown at 30°C for overnight in SD-2 and harvested by centrifuging at 5000 rpm for 10 min. Cell
218 pellets were resuspended in a lysis buffer (150mM NaCl, 10 mM HEPES, pH 7.5) with Pierce™
219 Protease Inhibitor (ThermoFisher Scientific #A32965) as suggested by the manual. Resuspended
220 cells were mixed with acid-washed glass beads (Sigma #G8772) and lysed by sonication for 5 min.
221 Soluble proteins were separated by centrifuging at 13000 rpm for 10 min, mixed with 3x laemmli
222 buffer, and resolved by SDS-PAGE gels and transferred to PVDF membranes (Bio-Rad #1620177)
223 for western blotting. Monoclonal ANTI-FLAG® M2-Peroxidase (HRP) antibody was used at 1:2000
224 (Millipore Sigma, A8592) dilution in a TBST buffer and incubated at 4°C overnight. Protein signals
225 were detected by using SuperSignal™ West Pico PLUS Chemiluminescent Substrate
226 (ThermoFisher Scientific #34580) and visualized by ChemiDoc™ Touch Gel Imaging System (Bio-
227 Rad).

228

229 ***Rice protoplast transformation and cell viability assay***

230 Protoplasts were prepared according to [33], with modifications. Seeds of the rice cultivar Kitaake
231 (*Oryza sativa*) were surface sterilized and grown on ½ MS media at 25°C in dark for 12 days before
232 transitioning to a photoperiod of 12 h light (approximately 150 µmol m-2 s-1) and of 12 h darkness

233 for two days. Rice plants were cut into approximately 1 mm strips and immediately transferred
234 into 0.6 M mannitol for 10 min in the dark.
235
236 The rice strips were then incubated with an enzyme solution (1.5% Cellulase RS, 0.75%
237 Macerozyme R-10, 0.6 M mannitol, 10 mM MES at pH 5.7, 10 mM CaCl2 and 0.1% BSA) for 5 h in
238 the dark with gentle shaking at 40 rpm. The enzymatic digestion was stopped by adding an equal
239 volume of W5 solution (154 mM NaCl, 125 mM $CaCl_2$, 5 mM KCl and 2 mM MES at pH 5.7),
240 followed by a gentle shaking by hands for 10 seconds. Protoplasts were released and washed
241 through 40 µm nylon mesh into round-bottom tubes three times using W5 solution. The washed
242 protoplasts were harvested by centrifugation at 380 g for 10 min, and pellets were resuspended
243 in MMG solution (0.4 M mannitol, 15 mM $MgCl_2$, and 4 mM MES at pH 5.7) at a concentration of
244 6×10^6 cells/mL, determined using a hematocytometer.
245
246 For protoplast transfection, 10 µg of plasmid DNA was mixed with 100 µL of the protoplasts and
247 100 µL freshly prepared PEG solution [40% (W/V) PEG 4000; Sigma, 0.2 M mannitol, and 0.1 M
248 $CaCl_2$]. The mixed samples were incubated in the dark for 20 min at room temperature. After
249 incubation, 2 mL W5 solution was added to stop the transfection, and protoplasts were pelleted
250 by centrifugation at 380 g for 10 min. The protoplasts were resuspended in 1 mL fresh W5 solution
251 and cultured in the dark for 16 h for cell viability assay or 4 h for detecting protein expression.
252
253 Protein expression from protoplasts were assayed by pull-down assay and Western blot. Four
254 individual transfection events (equals to 2.4×10^6 cells) were collected and harvested by
255 centrifugation at 380 g for 5 min. Cell pellets were resuspended with a lysis buffer (150 mM NaCl,
256 10 mM HEPES, pH 7.5) containing Pierce™ Protease Inhibitor (ThermoFisher Scientific #A32965)
257 as suggested by the manual. Cells were lysed by strong vortex for 5 min and mixed with 20 µL of
258 Pierce™ Anti-DYKDDDDK Magnetic Agarose (Thermo Scientific™, #A36797). The mixtures were
259 incubated at 4°C for two hours and wash for three times with the lysis buffer as suggested by the
260 manual. Samples were mixed with 3x laemmli buffer and resolved by SDS-PAGE gels and
261 transferred to PVDF membranes (Bio-Rad # 1620177) for immune blotting. Monoclonal ANTI-

262 FLAG® M2-Peroxidase (HRP) antibody (Millipore Sigma, A8592) was used at 1:2000 dilution in a
263 TBST buffer and incubated at 4°C for overnight. Protein signals were detected by using
264 SuperSignal™ West Pico PLUS Chemiluminescent Substrate (ThermoFisher Scientific #34580) and
265 visualized by ChemiDoc™ Touch Gel Imaging System (Bio-Rad).
266
267 ***Cell viability assay***
268 Protoplast cell viability was assayed using the CellTiter-Glo® 2.0 Cell Viability Assay kit (Promega,
269 #G9241) as instructed by the manual and by [34]. In brief, 100 µL of protoplasts resuspended in W5
270 were mixed with 100 µL of the CellTiter-Glo reagent in a 96-well white assay plate. The samples
271 were mixed at orbital shaker for five minutes and then incubated in the dark for 10 min at room
272 temperature prior to recording the luminescent signal. Luminescence was measured using the
273 TriStar LB 941 Multimode Microplate Reader and MikroWin 2000 software (Berthold).
274
275 ***RNA extraction and qPCR***
276 Total RNA was extracted from rice protoplasts seven hours after transfection by using the
277 PicoPure™ RNA Isolation Kit (ThermoFisher Scientific, #KIT0204) with on-column DNase
278 treatment as per manual instructed. First-strand cDNA was synthesized using M-MLV Reverse
279 Transcriptase (Promega, #M1701) with an oligo d(T) primer at 25 µg/mL. The transcripts of
280 defense marker genes were quantified by using iTaq™ Universal SYBR® Green One-Step Kit (BIO-
281 RAD, #1725150) with 40 cycles of 1 s at 95°C and 30 s at 60°C.
282
283 **Data analyses and availability**
284 For protoplast viability assays, at least five independent transfection events were used as
285 biological replicates, and the presented results are representative of at least three independent
286 experiments. For qPCR of defense gene activation, four independent transfection events were
287 used. Statistical differences were detected using one way ANOVA coupled with a Tukey HSD post-
288 hoc test, $\alpha = 0.05$. Protein assays including kinase activity tests, western blot, and yeast-two hybrid
289 were independently repeated at least twice with similar results. All materials are available from

the corresponding author upon request. Raw data underlying each figure are available at https://doi.org/10.5281/zenodo.11087676.

293 **Results**

294 ***RWT4 recognizes AvrPWT4 in wheat and rice***

295 *Rwt4* is located in the D genome of hexaploid wheat [21]. First, we phenotyped the hexaploid wheat
296 cultivars Norin 4 (*Rwt4*), Cadenza (*Rwt4*), Hope (*rwt4*), and Chinese Spring (*rwt4*) for their
297 responses to inoculation with spores of *M. oryzae* pathotype *Triticum* (MoT) isolate Br48 and its
298 *AvrPwt4* transformants. Disease symptoms were recorded four days post-inoculation (dpi).
299 Leaves infected with Br48 showed moderate to severe symptoms across all tested samples. As
300 expected, the Br48 transformant carrying *AvrPwt4* failed to cause comparable symptoms in
301 Norin4 and Cadenza, demonstrating that lines harboring *Rwt4* are resistant to *AvrPwt4*-carrying
302 strains (Figure 1A, Table S1). All genotypes we tested lack *Rmg8*, an MCTP-kinase that recognizes
303 another *M. oryzae* effector [35,36].

304

305 Next, we sought to identify a rapid plant system to investigate TKP activation. We employed a rice
306 protoplast system to transiently co-express *Rwt4* and *Pwt4* and assayed defense responses,
307 including cell death and defense gene expression (Figure 1B). Luminance-based cell viability
308 assays were conducted to evaluate the ability of *Rwt4* to specifically recognize *AvrPwt4* when
309 expressed in rice. Protoplasts co-expressing *AvrPwt4* and the resistant Cadenza allele of *Rwt4*
310 ($Rwt4^{Ca}$) exhibited a significant reduction in viability compared to cells transfected with $Rwt4^{Ca}$
311 plus an empty vector (Figure 1C, $p<0.0001$). In contrast, co-transfecting the susceptible Chinese
312 Spring allele of *Rwt4* ($Rwt4^{Cs}$) and *AvrPwt4* failed to cause cell death (Figure 1C). Furthermore, we
313 examined RWT4's specificity in recognizing PWT4 for defense activation by co-transfecting $Rwt4^{Ca}$
314 with either *AvrPwt4* or *VirPwt4* in rice protoplasts. A significant strong reduction of cell viability
315 was specifically observed in cells co-transfected with $Rwt4^{Ca}$ and *AvrPwt4* but not in cells co-
316 transfected with either *VirPwt4* or an empty vector (Figure 1D, $p<0.0001$). Similarly, we measured
317 defense gene activation and observed that the defense marker genes *RSOsPR10*, *OsPr10a* and
318 *OsRin4* [37-39] were specifically induced in cells co-transfected with $Rwt4^{Ca}$ and *AvrPwt4* (Figure 1E).
319 RWT4 and PWT4 effectors were detectable in rice protoplasts by western blot (Figure S1). These
320 results demonstrate that RWT4 is functional when transferred to rice and can specifically
321 recognize the AvrPWT4 effector.

322

323 ***The kinase activity of RWT4 is required for defense activation***

324 *Rwt4* was identified as a tandem kinase encoding a kinase-pseudokinase domain organization. To
325 explore the kinase domain family/subfamily of RWT4^{Ca}, we conducted a sequence homology
326 search for RWT4^{Ca} kinase domain (KD, 1-478) and pseudokinase domain (PKD, 540-914) in The
327 Arabidopsis Information Resource (TAIR, www.arabidopsis.org), identifying AT4G00960 and
328 AT4G23190 as orthologs for KD and PKD, respectively. Analysis of their kinase family/subfamily
329 using the annotated Arabidopsis kinome dataset [40] revealed that both of the domains belong to
330 the LRR_8B kinase subfamily, predominantly associated with cysteine-rich receptor-like kinases
331 for defense regulation. The two domains are interconnected by a linker region, which forms a
332 flexible intrinsic disorder (Figure 2A). Except for WTK1, all other identified TKPs controlling disease
333 resistance contain LRR-8B kinase domains [8,9,14].

334

335 We explored the importance of kinase activity in RWT4-mediated defense. We expressed and
336 purified RWT4 proteins including full length wild type RWT4^{Ca} (His-MBP-RWT4^{Ca}), its kinase
337 domain (His-MBP-KD), pseudokinase domain (His-MBP-PKD), and a kinase-dead variant (His-
338 MBP-RWT4$^{Ca_K217R/K327R}$), with mutations in the two conserved lysines located within the active
339 site (K217R) and ATP binding site (K327R) predicted via InterPro [41,42] (Figure 2B). Immunoblot
340 analysis employing a phosphor-Thr/Tyr antibody detected phosphorylated His-MBP-RWT4^{Ca} and
341 His-MBP-KD while the signal was removed by treatment with lambda protein phosphatase (Figure
342 2C), suggesting RWT4^{Ca} and His-MBP-KD are capable of autophosphorylation. In contrast, RWT4's
343 pseudokinase domain and MBP-RWT4$^{Ca_K217R/K327R}$ exhibited no detectable phosphorylation by
344 western blot (Figure 2C). Subsequent kinase assays using [^{32}P]γATP detected *de novo*
345 phosphorylation of His-MBP-RWT4^{Ca} and His-MBP-KD, whereas His-MBP-PKD and His-MBP-
346 RWT4$^{Ca_K217R/K327R}$ failed to exhibit kinase activity (Figure 2D). Western blot with anti-HIS and
347 Coomassie-stained SDS-PAGE analysis further revealed a size shift between His-MBP-RWT4^{Ca} and
348 His-MBP-RWT4$^{Ca_K217R/K327R}$ (Figure 2B and 2C), further confirming that RWT4$^{Ca_K217R/K327R}$ serves
349 as a kinase dead variant of RWT4^{Ca}. These data demonstrate that RWT4 is an active kinase and
350 contains kinase-pseudokinase domain architecture.

351

352 Next, we employed mass spectrometry to identify unique RWT4 phosphorylation sites upon
353 AvrPWT4 recognition. RWT4 was phosphorylated at multiple sites in the absence of AvrPWT4.
354 Four unique phosphorylated residues were identified only after incubation with recombinant
355 AvrPWT4, two located within the KD and two within the PKD (Figure S2, S3). One of these
356 phosphorylated residues, Y204, resides within the ATP binding loop of RWT4's KD and is a
357 conserved residue in the KD of other TKP LRR_8B members (Figure S3). The remaining three
358 residues, T164, S609, S803, are not conserved across the KD/PKD of other TKP LRR_8B members.
359

360 To determine if RWT4's kinase activity is required for defense induction, we co-transfected
361 *AvrPwt4* with either *Rwt4*^{Ca} or *Rwt4*$^{Ca_K217R/K327R}$ and measured cell viability as an indicator of
362 defense activation. Unlike wild type *Rwt4*^{Ca}, which strongly reduced cell viability when recognizing
363 *AvrPwt4*, cells co-transfected with *AvrPwt4* and *Rwt4*$^{Ca_K217R/K327R}$ exhibited no significant
364 decrease in cell viability (Figure 2E, $p<0.0001$). Western blot detected protein equal expression of
365 RWT4^{Ca} and RWT4$^{Ca_K217R/K327R}$ in rice protoplasts (Figure S1A). These data collectively
366 demonstrate that RWT4 kinase activity is necessary for defense responses mediated by
367 perception of AvrPWT4.
368

369 ***RWT4 phosphorylates AvrPWT4, but not the unrecognized effector VirPWT4***

370 Next, we sought to investigate whether RWT4 phosphorylates AvrPWT4. Purified His-MBP-
371 RWT4^{Ca} was mixed with GST-AvrPWT4 or GST-VirPWT4 at 1:1 molar ratio 30 min prior to the
372 kinase assay using [^{32}P]γATP. The common kinase substrate myelin basic protein (MyBP) was
373 included as a positive control. Phosphorylated GST-AvrPWT4 was detected from samples
374 incubated with His-MBP-RWT4^{Ca} (Figure 2F) or His-MBP-KD (Figure S4A). However, no
375 phosphorylated GST-AvrPWT4 was observed from samples incubated with His-MBP-PKD (Figure
376 S4A) or the kinase dead variant His-MBP-RWT4$^{Ca_K217R/K327R}$ (Figure S4B). Furthermore, RWT4^{Ca}
377 did not phosphorylate GST-VirPWT4 (Figure 2F). These findings demonstrate that RWT4^{Ca}
378 specifically transphosphorylates the recognized effector AvrPWT4.
379

380 To further investigate the biological significance of AvrPWT4 phosphorylation, we mapped
381 AvrPWT4 phosphorylation sites by mass-spectrometry and identified five phosphorylated
382 residues (Figure S5A). One phosphorylated residue, T45, is only found in AvrPWT4 (Figure S5B,
383 Figure 2G). We generated the phosphorylation null mutant *AvrPwt4*^{T45A} and tested its ability to
384 be recognized by RWT4^{Ca} in rice protoplasts. However, *AvrPwt4*^{T45A} had a similar ability to induce
385 cell death in protoplasts as wild-type *AvrPwt4* when co-transfected with *Rwt4*^{Ca}, suggesting the
386 effector phosphorylation at this residue is not required for RWT4-mediated defense (Figure 2G,
387 $p<0.0001$). Western blot detected AvrPWT4 and AvrPWT4^{T45A} expression from protoplasts (Figure
388 S5C).
389
390 ***RWT4^{Ca} directly and specifically interacts with AvrPWT4***
391 It has been an unsolved question if TKPs can act as a receptor for a corresponding effector. Yeast
392 two-hybrid demonstrated an interaction between RWT4^{Ca} and AvrPWT4 but no interaction with
393 VirPWT4 (Figure 3A). Western blot analysis confirmed the protein expression of RWT4^{Ca},
394 AvrPWT4, and VirPWT4 in yeast (Figure S6). To further validate that the RWT4 TKP can directly
395 interact with AvrPWT4, we utilized Bio-layer interferometry (BLI) to characterize binding kinetics.
396 RWT4^{Ca} was purified with a His-tag for immobilizing to the biosensors, while AvrPWT4 and
397 VirPWT4 were expressed with a GST tag which was subsequently removed by TEV protease
398 treatment during purification (Figure 3B). Based on the molecular weight and yields of purified
399 proteins, a 1.5x dilution of molar concentration gradient of effectors were prepared from 10 µM
400 to 51 nM as ligands, while purified His-RWT4^{Ca} was immobilized to the Octet NTA biosensors as
401 analytes. Strong binding kinetics between RWT4^{Ca} were observed for all tested concentrations of
402 AvrPWT4 showing wavelength shifts from 0.6844 nm to 0.0264 nm, with binding constants (K_D)
403 less than $1x10^{-12}$ (Figure 3C and Table S2). In contrast, the binding affinity of RWT4^{Ca} to VirPWT4
404 is weak and unstable, showing wavelength shifts from 0.1754 nm to 0.0023nm with a K_D value
405 greater than 10^{-7} (Figure 3C and Table S2). Background binding to GST exhibited similar weak
406 kinetics comparable to the binding observed between His-RWT4^{Ca} and VirPWT4 (Figure 3C and
407 Table S2). These results demonstrate that RWT4^{Ca} has direct, stable, and specific binding to
408 AvrPWT4.

409

410 Further BLI assays were conducted to determine which RWT4 ^{Ca} domain is required for AvrPWT4
411 interaction. Due to challenges in obtaining high-quality KD and PKD proteins with a His-tag, we
412 expressed proteins with a His-MBP tag to promote solubility. Interestingly, both His-MBP-KD and
413 His-MBP-PKD demonstrated measurable binding to AvrPWT4 within concentrations ranging from
414 10 µM to 173 nM, exhibiting similar binding constants although His-MBP-PKD displayed weaker
415 wavelength shifts (Figure 3D and Table S3). Notably, the full-length His-MBP-RWT4^{Ca} exhibited
416 stronger binding affinity than its individual domains, and all three tested proteins showed no
417 binding to GST (Figure 3D and Table S3). Collectively, these results indicate that RWT4 functions
418 as a receptor for AvrPWT4, with both KD and PKD involved in effector binding.

419

420 ***Structure-guided identification of RWT4 specificity***

421 We further investigated the sequence or structural features determining the binding of RWT4 to
422 AvrPWT4. By employing AlphaFold-Multimer [43], we predicted the structure of the RWT4-
423 AvrPWT4 protein complex (Figure 4A, left). Structural modeling suggests that AvrPWT4 (orange)
424 acts as a bridge between the KD (green) and PKD (blue). We identified two potential binding
425 regions in the KD (117-127, 261-270) and two regions in the PKD (551-560, 627-645). Next, we
426 compared *Rwt4* alleles from known *MoT*-resistant wheat cultivars (Norin 4, Cadenza, Jagger,
427 Paragon and Claire) with susceptible cultivars (Chinese Spring and CDC Stanley) [21,22] (Figure S7
428 and Table S4). We identified sequence polymorphisms within the predicted KD binding region 1
429 (117-127) and PKD region 2 (627-645) (Figure 4B). Additionally, a six-amino-acid extension at the
430 C-terminus was specifically conserved in susceptible *Rwt4* alleles (Figure 4B).

431

432 To test the importance of the identified binding regions from AlphaFold-Multimer and sequence
433 analyses, we generated RWT4 variants by replacing sequences between resistant and susceptible
434 alleles in the context of RWT4^{Ca} (RWT4^{Ca_Reg1}: V123LR124T, RWT4^{Ca_Reg2}: R627T) (Figure 4B). A
435 RWT4 variant incorporating the six-amino-acid extension at its C-terminus was also generated
436 (RWT4$^{Ca_+C\text{-}tail}$) (Figure 4B). Subsequently, we evaluated the capacity of these RWT4 variants to
437 perceive AvrPWT4 for defense activation in rice protoplasts. Protoplasts transfected with wild-

438 type *Rwt4*^{Ca} and *AvrPwt4* displayed a significant reduction in cell viability (Figure 4C). However,
439 cells transfected with the *Rwt4*^{Ca_Reg1} variant and *AvrPwt4* failed to show a decrease in viability
440 (Figure 4C). Similarly, no cell death was observed upon co-transfection of *Rwt4*$^{Ca_+C\text{-}tail}$ with
441 *AvrPwt4* (Figure 4C). Cells expressing *Rwt4*^{Ca_Reg2} and *AvrPwt4* exhibited a comparable reduction
442 in cell viability to cells expressing *Rwt4*^{Ca} and *AvrPwt4* (Figure 4C, $p<0.0001$). Western blotting
443 confirmed the protein expression of RWT4^{Ca}, RWT4^{Ca_Reg1}, RWT4^{Ca_Reg2}, and RWT4$^{Ca_C\text{-}tail}$ in rice
444 protoplasts (Figure S8A). These findings highlight the importance of RWT4^{Ca}'s C-terminus and
445 residues V124/R125 in the KD in defense activation (Figure 4A, right).
446
447 To assess the impact of these residues on AvrPWT4 binding, yeast-two hybrid analyses was
448 conducted. As expected, RWT4^{Ca} can interact with AvrPWT4 (Figure 4D and S8B). However, a
449 weak interaction was observed between the susceptible variant from Chinese Spring, RWT4^{Cs},
450 and AvrPWT4 (Figure S8B). Next, we analyzed the interaction between RWT4 variant proteins and
451 AvrPWT4. No interaction was observed between RWT4^{Ca_Reg1} and AvrPWT4, indicating that
452 V124/R125 is required for AvrPWT4 binding (Figure 4D). The C-terminal extension did not
453 influence binding to AvrPWT4 (Figure 4d). Western blot assays confirmed expression of RWT4 and
454 its variants in yeast (Figure S8C). These data demonstrate that the binding capacity of RWT4 to
455 AvrPWT4 is a critical determinant of eliciting defense.
456

457 **Discussion**

458 TKPs have emerged as a novel class of non-canonical resistance proteins, representing ~10% of
459 the cloned *Triticeae* R genes [4,44]. Currently, TKPs conferring disease-resistance are exclusively
460 found in monocots [6]. In this study, we demonstrate the RWT4 TKP can be transferred and elicit
461 defense between wheat and rice. Furthermore, both RWT4 kinase activity and direct effector
462 binding are required for defense activation. It was hypothesized that TKP pseudokinase domains
463 acts as a decoy for effector binding, activating the kinase domain for downstream
464 phosphorylation or signaling [8]. Our results demonstrate that AvrPWT4 binds to both KD and PKD.
465 AvrPWT4 binding to both domains *in planta* may facilitate RWT4 intramolecular kinase
466 interactions for activation (Figure 4E). For plant receptor-like kinases, hetero-dimerization is a
467 common activation mechanism for signaling initiation [45].

468

469 TKP-mediated resistance is associated with the induction of cell death and robust defense
470 responses [6,13,20]. Like PRR and NLR immune receptors that can directly detect pathogen
471 components, RWT4 directly binds to AvrPWT4 and this binding is crucial for defense activation.
472 *Rwt3* is allelic to *Wtk3*, which confers resistance to powdery mildew disease caused by *Blumeria*
473 *graminis* f.sp. *tritici* [13,21]. Though highly similar in amino acid sequence, the effector targets of
474 WTK3 are currently unknown, and no ortholog of *Pwt4* is present in *B. graminis*. The majority of
475 functional TKPs conferring disease resistance belong to the LRR_8B kinase subfamily [8,9,14].
476 Prototypic members of this subfamily are cysteine-rich receptor-like kinases involved in plant
477 defense and can confer resistance to fungal pathogens [46,47]. Collectively, our results are consistent
478 with the hypothesis that TKPs represent a novel class of immune receptors and directly lead to
479 phosphorylation of defense regulators. Although it is possible that an NLR or PRR may be required
480 for TKP signaling, this is not the most parsimonious explanation. No NLRs or PRRs have been
481 identified as necessary for TKP function in initial mapping or subsequent EMS screening [6,9,13,21].
482 While RWT4 is genetically linked to an NLR, EMS mutagenesis of that NLR did not abrogate
483 resistance [21]. Furthermore, RWT4 is transferable between wheat and rice, retaining effector
484 recognition. The elucidation of TKP immune complexes and direct phosphorylation targets will
485 reveal how these novel proteins confer resistance.

486

487 *In vitro* kinase activity has been demonstrated for RPG1, WTK7-Tm, and our work on the RWT4
488 TKP [9,17]. *In vitro*, the PKD does not inhibit the kinase activity of RPG1 and RWT4 [17]. We hypothesize
489 that kinase activity is inhibited at a resting state *in planta* in the absence of pathogen perception.
490 RPG1 activation *in planta* is only observed in the presence of avirulent spores of *P. graminis* [18],
491 consistent with the hypothesis that TKPs rely on pathogen perception for activation. Additional
492 regions are also required for RWT4 full functionality such as the V123R124 sites for effector
493 binding and the C-terminus (Figure 4c and 4d).

494

495 Effector targeting of plant kinases is an important strategy to enhance pathogen virulence. The
496 *Pseudomonas syringae* AvrPtoB effector targets the plant kinase SnRK2.8, promoting pathogen
497 virulence upon SnRK2.8 phosphorylation [48]. The fungal NIS1 effector family from *Colletotrichum*
498 *spp*. and *Magnaporthe oryzae* act as kinase inhibitors, targeting the BAK1 and BIK1 kinases
499 required for effective defense mediated by multiple surface-localized receptors [49]. PWT4 has
500 canonical fugal effector features, including an N-terminal secretion signal and small size (75 amino
501 acids) [22]. AvrPWT4 suppresses resistance conferred by RMG8, an MCTP kinase fused with multiple
502 C2 domains [35,50]. Thus, AvrPWT4 likely targets plant kinases to promote virulence in the absence
503 of RWT4. Accordingly, we hypothesize that KFPs serve both as receptors and decoys for
504 perception and deception of biotrophic fungal effectors that are aiming to suppress host kinases
505 involved in the activation of plant immunity [5].

506

507 TKPs have emerged as a novel class of resistance proteins that have been widely deployed to
508 control devastating biotrophic fungal pathogens [6,9,10,13,21]. Future investigations identifying
509 effector-TKP pairs as well as their phosphorylation targets will shed light into TKP activation and
510 signaling. This foundational information can facilitate receptor engineering and the deployment
511 of TKPs across diverse plant species.

512

513

514

Acknowledgements:

This research is supported by grants from the United States National Science Foundation (1937855) and the United States Department of Agriculture (2020-67013-32577) to GC and the United States-Israel Binational Science Foundation (BSF, 2019654) to TF. MS analysis was carried out at the Genomics Center Proteomics Core at the University of California, Davis. The kinase assay using [^{32}P]γATP was conducted in the facility established by Dr. Yen-Wen Kuo, Department of Plant Pathology at the University of California, Davis. BLI experiments were performed in the Cortopassi Lab with technical assistance from Dr. Alexey Tomilov at the University of California, Davis. Rice Kitaake seeds were provided by Dr. Pamela Ronald, Department of Plant Pathology at the University of California, Davis. The pUC19::Zm*UBI* plasmid was provided by Dr. Jorge Dubcovsky from the Department of Plant Science, University of California, Davis. The pET28s::GST vector was provided by Dr. Nitzan Shabek, Department of Plant Biology, University of California, Davis.

Author contributions

Y-CS and GC designed the study with assistance from TZ. SA performed wheat inoculation experiments, YL performed yeast-two hybrid, SB assisted with molecular cloning and western blotting under the guidance of Y-CS and GC. Y-CS performed all other experiments and data analyses. Y-CS and GC wrote the original draft and all authors reviewed and edited the manuscript.

Declaration of interests

The authors declare no competing interests.

538 **References:**

539 1 Dodds, P. N. & Rathjen, J. P. Plant immunity: towards an integrated view of plant-pathogen
540 interactions. *Nat Rev Genet* **11**, 539-548 (2010). https://doi.org:10.1038/nrg2812
541 2 Chiang, Y.-H. & Coaker, G. Effector Triggered Immunity: NLR Immune Perception and
542 Downstream Defense Responses. *The Arabidopsis Book* **2015** (2015).
543 3 Couto, D. & Zipfel, C. Regulation of pattern recognition receptor signalling in plants. *Nat*
544 *Rev Immunol* **16**, 537-552 (2016). https://doi.org:10.1038/nri.2016.77
545 4 Sanchez-Martin, J. & Keller, B. NLR immune receptors and diverse types of non-NLR
546 proteins control race-specific resistance in Triticeae. *Curr Opin Plant Biol* **62**, 102053
547 (2021). https://doi.org:10.1016/j.pbi.2021.102053
548 5 Fahima, T. & Coaker, G. Pathogen perception and deception in plant immunity by kinase
549 fusion proteins. *Nat Genet* **55**, 908-909 (2023). https://doi.org:10.1038/s41588-023-
550 01396-w
551 6 Klymiuk, V. *et al.* Cloning of the wheat Yr15 resistance gene sheds light on the plant
552 tandem kinase-pseudokinase family. *Nat Commun* **9**, 3735 (2018).
553 https://doi.org:10.1038/s41467-018-06138-9
554 7 Yu, G. *et al.* Aegilops sharonensis genome-assisted identification of stem rust resistance
555 gene Sr62. *Nat Commun* **13**, 1607 (2022). https://doi.org:10.1038/s41467-022-29132-8
556 8 Klymiuk, V., Coaker, G., Fahima, T. & Pozniak, C. J. Tandem Protein Kinases Emerge as New
557 Regulators of Plant Immunity. *Mol Plant Microbe Interact* **34**, 1094-1102 (2021).
558 https://doi.org:10.1094/MPMI-03-21-0073-CR
559 9 Li, M. *et al.* A membrane associated tandem kinase from wild emmer wheat confers
560 broad-spectrum resistance to powdery mildew. *Nat Commun* **15**, 3124 (2024).
561 https://doi.org:10.1038/s41467-024-47497-w
562 10 Brueggeman, R. *et al.* The barley stem rust-resistance gene Rpg1 is a novel disease-
563 resistance gene with homology to receptor kinases. *Proc Natl Acad Sci U S A* **99**, 9328-
564 9333 (2002). https://doi.org:10.1073/pnas.142284999
565 11 Chen, S. *et al.* Wheat gene Sr60 encodes a protein with two putative kinase domains that
566 confers resistance to stem rust. *New Phytol* **225**, 948-959 (2020).
567 https://doi.org:10.1111/nph.16169
568 12 Gaurav, K. *et al.* Population genomic analysis of Aegilops tauschii identifies targets for
569 bread wheat improvement. *Nat Biotechnol* (2021). https://doi.org:10.1038/s41587-021-
570 01058-4
571 13 Lu, P. *et al.* A rare gain of function mutation in a wheat tandem kinase confers resistance
572 to powdery mildew. *Nat Commun* **11**, 680 (2020). https://doi.org:10.1038/s41467-020-
573 14294-0
574 14 Wang, Y. *et al.* An unusual tandem kinase fusion protein confers leaf rust resistance in
575 wheat. *Nat Genet* **55**, 914-920 (2023). https://doi.org:10.1038/s41588-023-01401-2
576 15 Yu, G. *et al.* The wheat stem rust resistance gene Sr43 encodes an unusual protein kinase.
577 *Nat Genet* **55**, 921-926 (2023). https://doi.org:10.1038/s41588-023-01402-1
578 16 Marchal, C., Michalopoulou, V. A., Zou, Z., Cevik, V. & Sarris, P. F. Show me your ID: NLR
579 immune receptors with integrated domains in plants. *Essays Biochem* **66**, 527-539 (2022).
580 https://doi.org:10.1042/Ebc20210084

17 Nirmala, J. *et al.* Subcellular localization and functions of the barley stem rust resistance receptor-like serine/threonine-specific protein kinase Rpg1. *Proc Natl Acad Sci U S A* **103**, 7518-7523 (2006). https://doi.org:10.1073/pnas.0602379103

18 Nirmala, J., Drader, T., Chen, X., Steffenson, B. & Kleinhofs, A. Stem rust spores elicit rapid RPG1 phosphorylation. *Mol Plant Microbe Interact* **23**, 1635-1642 (2010). https://doi.org:10.1094/MPMI-06-10-0136

19 Lolle, S., Stevens, D. & Coaker, G. Plant NLR-triggered immunity: from receptor activation to downstream signaling. *Curr Opin Immunol* **62**, 99-105 (2020). https://doi.org:10.1016/j.coi.2019.12.007

20 Nirmala, J. *et al.* Concerted action of two avirulent spore effectors activates Reaction to Puccinia graminis 1 (Rpg1)-mediated cereal stem rust resistance. *Proc Natl Acad Sci U S A* **108**, 14676-14681 (2011). https://doi.org:10.1073/pnas.1111771108

21 Arora, S. *et al.* A wheat kinase and immune receptor form host-specificity barriers against the blast fungus. *Nat Plants* **9**, 385-392 (2023). https://doi.org:10.1038/s41477-023-01357-5

22 Inoue, Y. *et al.* Evolution of the wheat blast fungus through functional losses in a host specificity determinant. *Science* **357**, 80-83 (2017). https://doi.org:10.1126/science.aam9654

23 Hossain, M. M. Wheat blast: A review from a genetic and genomic perspective. *Front Microbiol* **13**, 983243 (2022). https://doi.org:10.3389/fmicb.2022.983243

24 Tagle, A. G., Chuma, I. & Tosa, Y. Rmg7, a New Gene for Resistance to Triticum Isolates of Pyricularia oryzae Identified in Tetraploid Wheat. *Phytopathology* **105**, 495-499 (2015). https://doi.org:10.1094/PHYTO-06-14-0182-R

25 Hyon, G. S. *et al.* Characterization of interactions between barley and various host-specific subgroups of *Magnaporthe oryzae* and *M-grisea*. *J Gen Plant Pathol* **78**, 237-246 (2012). https://doi.org:10.1007/s10327-012-0386-6

26 Currinn, H., Guscott, B., Balklava, Z., Rothnie, A. & Wassmer, T. APP controls the formation of PI(3,5)P(2) vesicles through its binding of the PIKfyve complex. *Cell Mol Life Sci* **73**, 393-408 (2016). https://doi.org:10.1007/s00018-015-1993-0

27 Eschenfeldt, W. H., Lucy, S., Millard, C. S., Joachimiak, A. & Mark, I. D. A family of LIC vectors for high-throughput cloning and purification of proteins. *Methods Mol Biol* **498**, 105-115 (2009). https://doi.org:10.1007/978-1-59745-196-3_7

28 Shabek, N. *et al.* Structural insights into DDA1 function as a core component of the CRL4-DDB1 ubiquitin ligase. *Cell Discov* **4** (2018). https://doi.org:https://doi.org/10.1038/s41421-018-0064-8

29 Lin, Z. J., Liebrand, T. W., Yadeta, K. A. & Coaker, G. PBL13 Is a Serine/Threonine Protein Kinase That Negatively Regulates Arabidopsis Immune Responses. *Plant Physiol* **169**, 2950-2962 (2015). https://doi.org:10.1104/pp.15.01391

30 Demichev, V., Messner, C. B., Vernardis, S. I., Lilley, K. S. & Ralser, M. DIA-NN: neural networks and interference correction enable deep proteome coverage in high throughput. *Nat Methods* **17**, 41-44 (2020). https://doi.org:10.1038/s41592-019-0638-x

31 MacLean, B. *et al.* Skyline: an open source document editor for creating and analyzing targeted proteomics experiments. *Bioinformatics* **26**, 966-968 (2010). https://doi.org:10.1093/bioinformatics/btq054

625 32 Shah, N. B. & Duncan, T. M. Bio-layer interferometry for measuring kinetics of protein-
626 protein interactions and allosteric ligand effects. *J Vis Exp*, e51383 (2014).
627 https://doi.org:10.3791/51383
628 33 He, F., Chen, S., Ning, Y. & Wang, G. L. Rice (Oryza sativa) Protoplast Isolation and Its
629 Application for Transient Expression Analysis. *Curr Protoc Plant Biol* **1**, 373-383 (2016).
630 https://doi.org:10.1002/cppb.20026
631 34 Wang, J. *et al.* Reconstitution and structure of a plant NLR resistosome conferring
632 immunity. *Science* **364** (2019). https://doi.org:10.1126/science.aav5870
633 35 O'Hara, T. *et al.* The wheat powdery mildew resistance gene Pm4 also confers
634 resistance to wheat blast. *bioRxiv*, 2023.2009.2026.559489 (2023).
635 https://doi.org:10.1101/2023.09.26.559489
636 36 Asuke, S. *et al.* Evolution of wheat blast resistance gene Rmg8 accompanied
637 by differentiation of variants recognizing the powdery mildew fungus. *bioRxiv*,
638 2023.2009.2026.559445 (2023). https://doi.org:10.1101/2023.09.26.559445
639 37 De Kesel, J., Gomez-Rodriguez, R., Bonneure, E., Mangelinckx, S. & Kyndt, T. The Use of
640 PTI-Marker Genes to Identify Novel Compounds that Establish Induced Resistance in Rice.
641 *Int J Mol Sci* **21** (2020). https://doi.org:10.3390/ijms21010317
642 38 Huang, L. F. *et al.* Multiple Patterns of Regulation and Overexpression of a Ribonuclease-
643 Like Pathogenesis-Related Protein Gene, OsPR10a, Conferring Disease Resistance in Rice
644 and Arabidopsis. *PLoS One* **11**, e0156414 (2016).
645 https://doi.org:10.1371/journal.pone.0156414
646 39 Takeuchi, K. *et al.* RSOsPR10 expression in response to environmental stresses is regulated
647 antagonistically by jasmonate/ethylene and salicylic acid signaling pathways in rice roots.
648 *Plant Cell Physiol* **52**, 1686-1696 (2011). https://doi.org:10.1093/pcp/pcr105
649 40 Zulawski, M., Schulze, G., Braginets, R., Hartmann, S. & Schulze, W. X. The Arabidopsis
650 Kinome: phylogeny and evolutionary insights into functional diversification. *Bmc*
651 *Genomics* **15** (2014). https://doi.org:https://doi.org/10.1186/1471-2164-15-548
652 41 Piya, S. *et al.* Kinase-dead mutation: A novel strategy for improving soybean resistance to
653 soybean cyst nematode Heterodera glycines. *Mol Plant Pathol* **23**, 417-430 (2022).
654 https://doi.org:10.1111/mpp.13168
655 42 Paysan-Lafosse, T. *et al.* InterPro in 2022. *Nucleic Acids Res* **51**, D418-D427 (2023).
656 https://doi.org:10.1093/nar/gkac993
657 43 Evans, R. *et al.* Protein complex prediction with AlphaFold-Multimer. *bioRxiv*,
658 2021.2010.2004.463034 (2022). https://doi.org:10.1101/2021.10.04.463034
659 44 Chen, R., Gajendiran, K. & Wulff, B. B. H. R we there yet? Advances in cloning resistance
660 genes for engineering immunity in crop plants. *Current Opinion in Plant Biology* **77**,
661 102489 (2024). https://doi.org:https://doi.org/10.1016/j.pbi.2023.102489
662 45 Bender, K. W. & Zipfel, C. Paradigms of receptor kinase signaling in plants. *Biochem J* **480**,
663 835-854 (2023). https://doi.org:10.1042/BCJ20220372
664 46 Saintenac, C. *et al.* A wheat cysteine-rich receptor-like kinase confers broad-spectrum
665 resistance against Septoria tritici blotch. *Nat Commun* **12**, 433 (2021).
666 https://doi.org:10.1038/s41467-020-20685-0

667 47 Yadeta, K. A. *et al.* A Cysteine-Rich Protein Kinase Associates with a Membrane Immune
668 Complex and the Cysteine Residues Are Required for Cell Death. *Plant Physiol* **173**, 771-
669 787 (2017). https://doi.org:10.1104/pp.16.01404
670 48 Lei, L., Stevens, D. M. & Coaker, G. Phosphorylation of the Pseudomonas Effector AvrPtoB
671 by Arabidopsis SnRK2.8 Is Required for Bacterial Virulence. *Mol Plant* **13**, 1513-1522
672 (2020). https://doi.org:10.1016/j.molp.2020.08.018
673 49 Irieda, H. *et al.* Conserved fungal effector suppresses PAMP-triggered immunity by
674 targeting plant immune kinases. *Proc Natl Acad Sci U S A* **116**, 496-505 (2019).
675 https://doi.org:10.1073/pnas.1807297116
676 50 Inoue, Y., Vy, T. T. P., Tani, D. & Tosa, Y. Suppression of wheat blast resistance by an effector
677 of Pyricularia oryzae is counteracted by a host specificity resistance gene in wheat. *New*
678 *Phytol* **229**, 488-500 (2021). https://doi.org:10.1111/nph.16894
679

680

681 **Figures and figure legends**

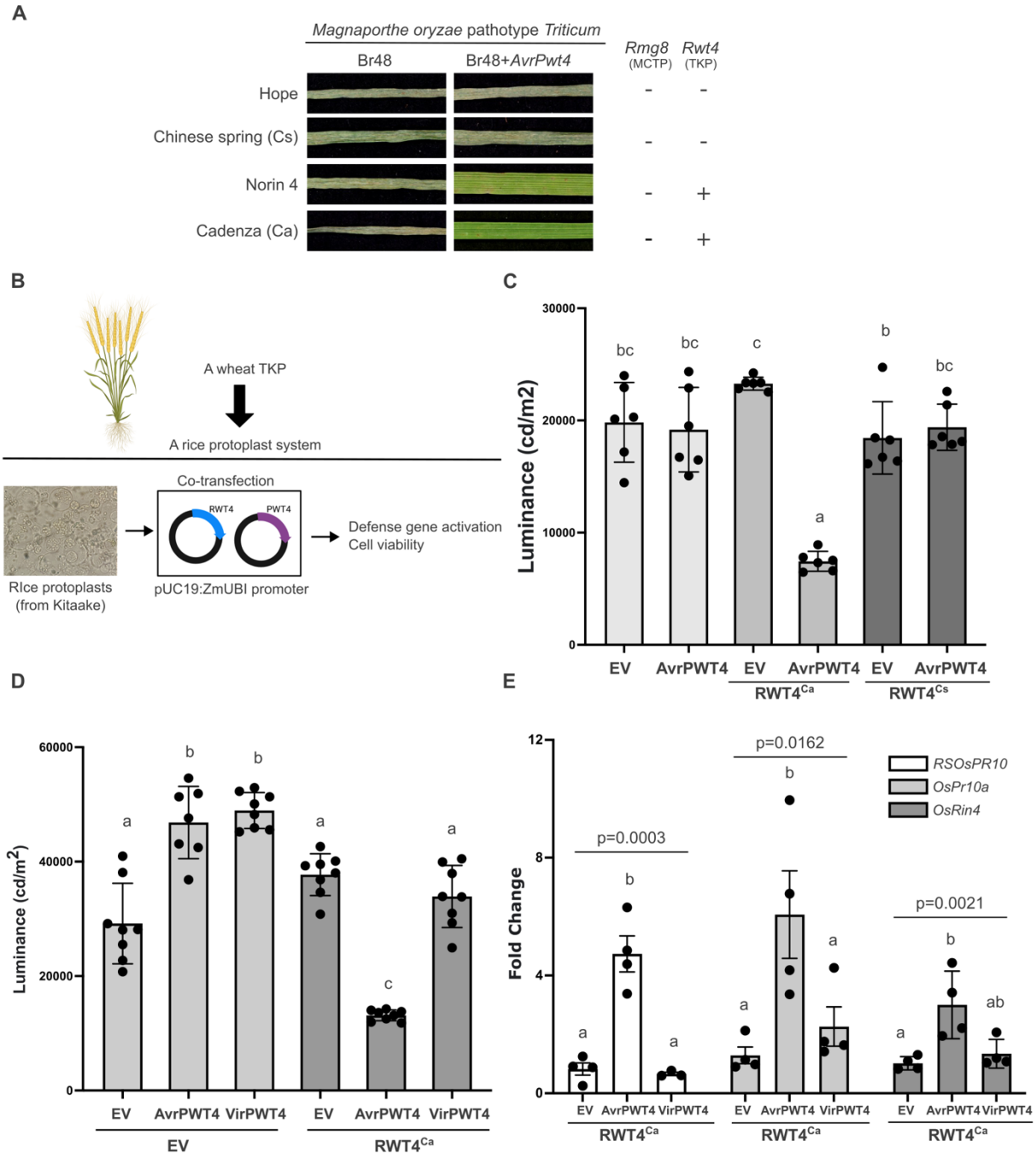

682

683 **Figure 1. RWT4-mediated resistance requires AvrPWT4 perception. (A)** Disease phenotyping of
684 wheat cultivars Hope, Chinese Spring (Cs), Norin 4, and Cadenza (Ca) with *Magnaporthe oryzae*
685 pathotype *Triticum* Br48 and a Br48 transformant carrying *AvrPwt4* (Br48+ *AvrPwt4*). Wheat
686 genotypes with (+) or without (-) functional *Rmg8* or *Rwt4* alleles are indicated. **(B)** Experimental
687 procedure of a rice protoplast transfection system for cell viability assays and defense gene

688 expression tests. Genes of interest (*Rwt4* or *Pwt4*) were cloned to a pUC19 vector containing a
689 maize polyubiquitin-1 (*Zm*Ubi-1) promoter. **(C)** RWT4 perceives AvrPWT4 triggering cell death
690 responses in rice protoplasts. RWT4 from Cadenza (Ca) and Chinese Spring (Cs) were assayed for
691 their perception of AvrPWT4 in rice protoplasts. Cell viability was measured as ATP activity
692 presented in luminance (cd/m^2). Luminescence (cd/m^2) was measured 16 h after protoplast
693 transfection. Six independent protoplast transfection events were used as biological replicates.
694 Mean±SEM are presented. Differences between treatments were analyzed using one-way ANOVA
695 with post-hoc Tukey HSD, $p<0.05$ **(D)** Only the recognized AvrPWT4 effector can induce RWT4^{Ca}-
696 triggered cell death. *Rwt4^{Ca}* was co-transfected with either the avirulent (*AvrPwt4*) or the virulent
697 (*VirPwt4*) allele of *Pwt4* in rice protoplasts. Protoplasts transfected with empty vector (EV) or co-
698 transfected with empty vector and *Pwt4* were treated as experimental controls. Experiments
699 were performed and analyzed as described in (C). **(E)** RWT4^{Ca} recognition of AvrPWT4 activates
700 defense gene expression. Expression fold change of *RSOsPR10* (Os12g36830), *OsPr10a*
701 (Os12g36850) and *OsRin4* (Os04g0379600) defense genes were measured 7 h after protoplast
702 transfection. Gene expression was normalized to the internal control *OsUbq5* (Os01g22490), and
703 data were normalized to the samples transfected with *Rwt4^{Ca}*+EV as expression fold changes.
704 Mean±SEM from four transfection events is presented. Differences between treatments were
705 analyzed using one-way ANOVA with post-hoc Tukey HSD, $p<0.05$.
706
707
708
709

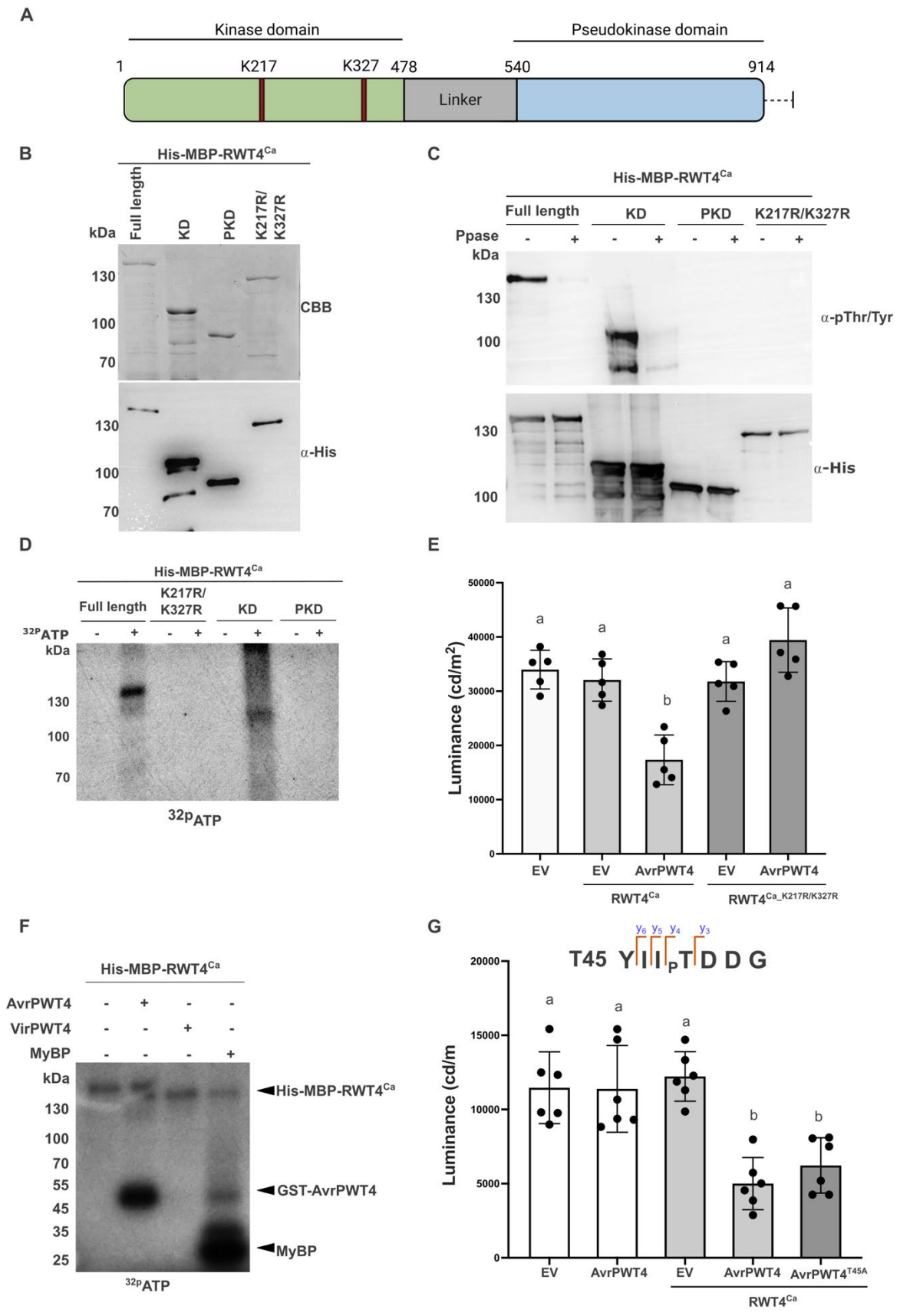
A
Kinase domain
Pseudokinase domain
1
K217
K327
478
540
914
Linker
B
His-MBP-RWT4Ca
Full length
KD
PKD
K217R/ K327R
kDa
130
100
70
CBB
α-His
C
His-MBP-RWT4Ca
Full length
KD
PKD
K217R/K327R
Ppase
kDa
α-pThr/Tyr
α-His
D
His-MBP-RWT4Ca
Full length
K217R/ K327R
KD
PKD
32PATP
kDa
32pATP
E
Luminance (cd/m2)
EV
AvrPWT4
RWT4Ca
RWT4Ca_K217R/K327R
F
His-MBP-RWT4Ca
AvrPWT4
VirPWT4
MyBP
kDa
His-MBP-RWT4Ca
GST-AvrPWT4
MyBP
32pATP
G
T45 YIIpTDDG
Luminance (cd/m
EV
AvrPWT4
AvrPWT4T45A
RWT4Ca

710

711 **Figure 2. RWT4 is an active kinase and transphosphorylates AvrPWT4. (A)** RWT4^{Ca} domain
712 organization. Kinase domain: 1-478 amino acid, green. Pseudokinase domain: 540-915 amino acid,
713 blue. Linker: 478-540 amino acid, grey. Predicted kinase active sites: K217 and K327. Dash: C-
714 terminal tail. **(B)** Purity of recombinant proteins isolated from *E. coli.* His-MBP-RWT4^{Ca}, kinase
715 domain (His-MBP-KD) pseudokinase domain (His-MBP-PKD), and its kinase dead variant
716 (RWT4$^{Ca_K217R/K327R}$) are shown by Coomassie brilliant blue (CBB) stained SDS-PAGE and
717 corresponding western blot using anti-His. **(C)** Autophosphorylation activity of His-MBP-RWT4^{Ca}.
718 Autophosphorylation status of the His-MBP-RWT4^{Ca} proteins were assayed by western blot using
719 anti-phospho-Threonine/Tyrosine antibody (α-pThr/Tyr) with or without lambda protein
720 phosphatase incubation prior to separating by SDS-PAGE. Anti-His western blotting (α-His)
721 demonstrates equal loading of the His-MBP-RWT4^{Ca} proteins. **(D)** Active protein phosphorylation
722 was measured by incubating the His-MBP-CaRWT4 proteins with [γ^{-32P}]ATP before separating by
723 SDS-PAGE and visualizing by autoradiography. **(E)** RWT4^{Ca}-AvrPWT4 triggered cell death requires
724 RWT4^{Ca} kinase activity. *Rwt4^{Ca}* and the kinase dead variant (*Rwt4^{Ca}*$_{K217R/K327R}$) were co-
725 transfected with *AvrPwt4* into rice protoplasts for cell viability assays. Five independent
726 protoplast transfection events were used as biological replicates and Mean±SEM are presented.
727 Treatment differences were analyzed using one-way ANOVA with post-hoc Tukey HSD, $p<0.05$. **(F)**
728 RWT4^{Ca} specifically trans-phosphorylates AvrPWT4. Transphosphorylation activity was assayed by
729 mixing His-MBP-RWT4^{Ca} and AvrPWT4 at room temperature for 20 min before incubated with [γ-
730 ^{32}P]ATP. Phosphorylation of the substrate proteins (AvrPWT4 or MyBP) were visualized via
731 autoradiography. **(G)** Phosphorylated peptides were mapped to the sequence of AvrPWT4 for
732 functional analysis. The phosphorylated peptide YIITDDG was identified from LC-MS/MS with the
733 phosphorylation site T45. *Rwt4^{Ca}* was co-transfected with either wild-type *AvrPwt4* or the
734 phosphorylation null mutant *AvrPwt4^{T45A}* to rice protoplasts. Luminescence (cd/m^2) was
735 measured 16 h after protoplast transfection as an indicator of cell viability. Six independent
736 protoplast transfection events were used as biological replicates. Mean±SEM are presented.
737 Differences between treatments were analyzed using one-way ANOVA with post-hoc Tukey HSD,
738 $p<0.05$.
739

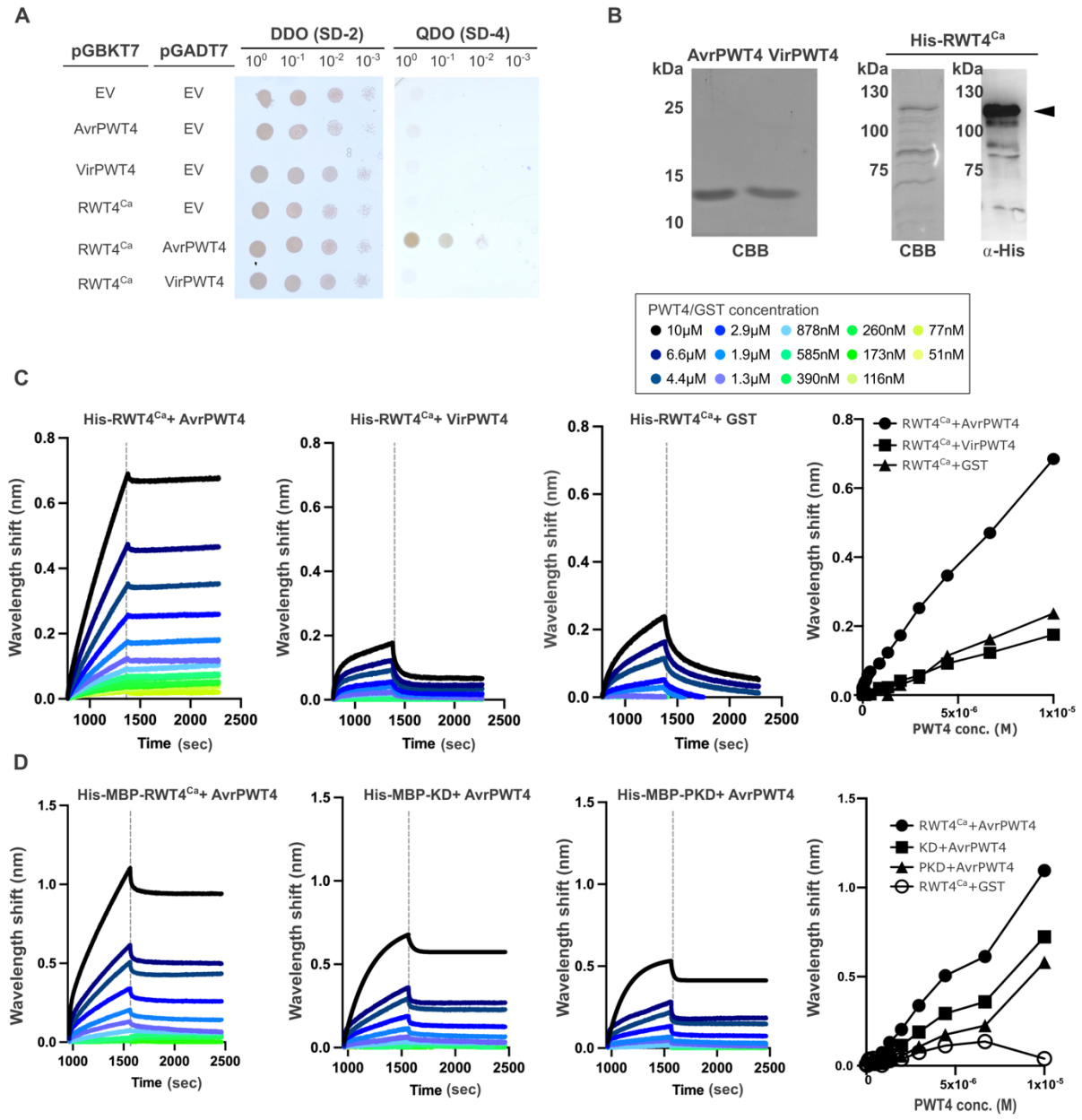

Figure 3. RWT4^{Ca} directly and specifically binds AvrPWT4. (A) Yeast-two hybrid (Y2H) assays using *Rwt4^{Ca}*, *AvrPwt4* and *VirPwt4*. *Rwt4^{Ca}* was cloned to the bait vector pGBKT7, while *AvrPwt4* and *VirPwt4* were cloned into the prey vector pGADT7. Yeast growth on DDO (SD-Leu/-Trp) media indicates the presence of the two plasmids, and the growth on QDO/X/A (SD-Ade/-His/-Leu/-

748 Trp/3-amino-1,2,4-triazole) media indicates interaction. Serial dilutions from cell suspensions of
749 a single yeast colony expressing the bait and prey plasmids are shown and represent the strength
750 of interaction. Empty vectors (EV) of pGBKT7 and pGADT7 were used as negative controls. **(B)**
751 Purity of AvrPWT4, VirPWT4, and His-RWT4^{Ca}. AvrPWT4 and VirPWT4 were expressed and
752 purified with a GST tag that was removed and separated by TEV protease and gel filtration. Purity
753 of His-CaRWT4 is shown by Coomassie brilliant blue (CBB) stained SDS-PAGE and Anti-His western
754 blotting (α-His). **(C)** and **(D)** Bio-layer interferometry (BLI) characterizes binding affinity between
755 His-RWT4^{Ca} and PWT4 proteins. **(C)** His-RWT4^{Ca} was mobilized to Ni-NTA biosensors as analytes
756 and incubated with a range of concentrations (51 nM to 10 µM) of AvrPWT4, VirPWT4, or GST
757 ligand proteins. Sensorgrams show BLI traces (wavelength shifts) during association and
758 dissociation steps (shown as time at the x-axis) normalized to no-ligand controls. The steady state
759 analysis (right) shows wavelength shifts against different ligand concentrations (AvrPWT4,
760 VirPWT4, or GST, from 10 µM to 116 nM). **(D)** His-MBP-RWT4^{Ca}, His-MBP-KD and His-MBP-PKD
761 proteins were immobilized to Ni-NTA biosensors and incubated with AvrPWT4. Binding affinity
762 between His-MBP-RWT4^{Ca}, His-MBP-KD and His-MBP-PKD to AvrPWT4 were detected by BLI
763 during association and dissociation steps (shown as time at the x-axis) and presented in the steady
764 state analysis against different concentrations of AvrPWT4 (right).
765

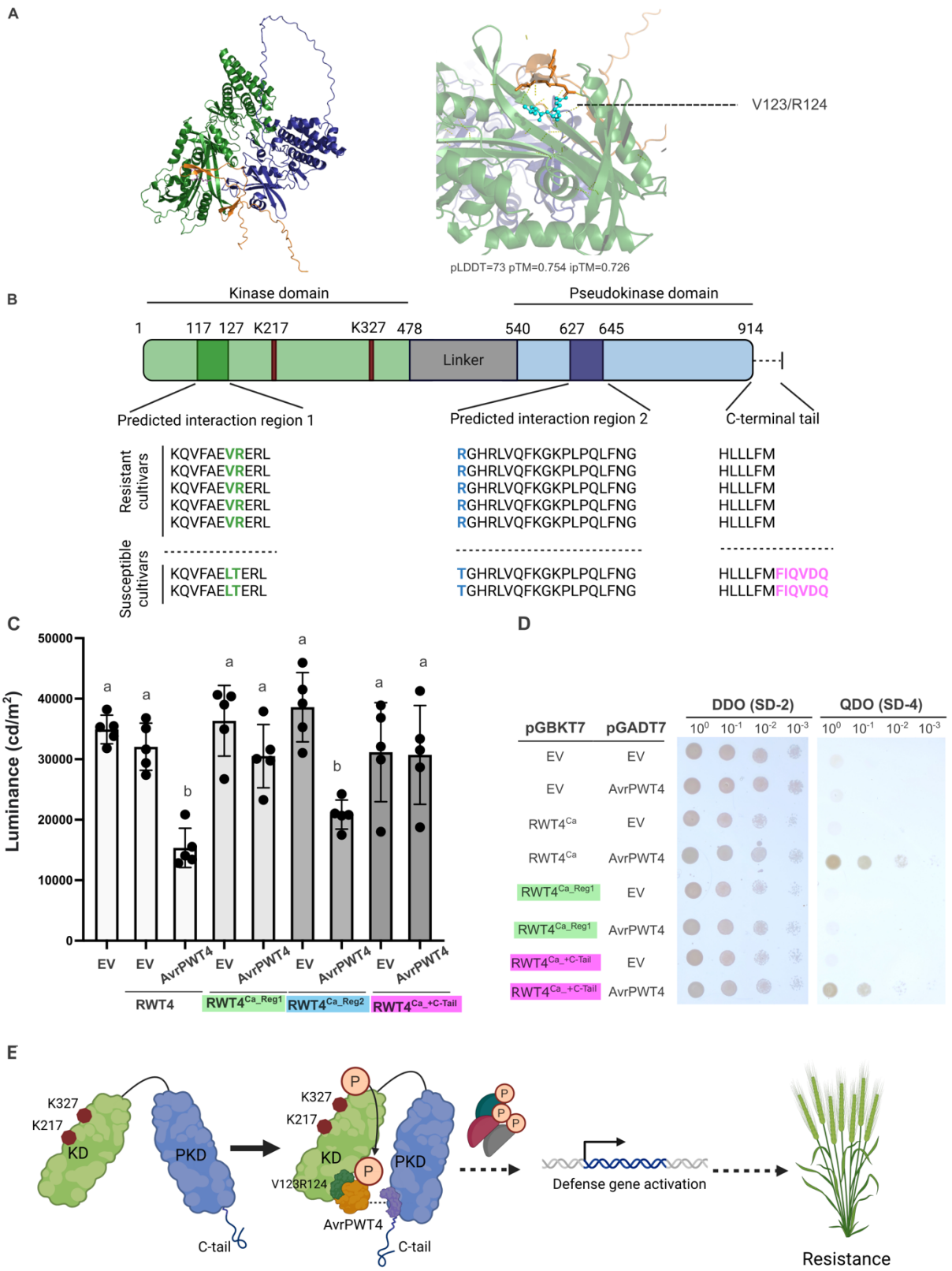
A
V123/R124
pLDDT=73 pTM=0.754 ipTM=0.726
B
Kinase domain
Pseudokinase domain
1
117
127
K217
K327
478
540
627
645
914
Linker
Predicted interaction region 1
Predicted interaction region 2
C-terminal tail
Resistant cultivars
KQVFAEVRERL
RGHRLVQFKGKPLPQLFNG
HLLLFM
Susceptible cultivars
KQVFAELTERL
TGHRLVQFKGKPLPQLFNG
HLLLFMFIQVDQ
C
Luminance (cd/m²)
50000
40000
30000
20000
10000
0
EV
AvrPWT4
RWT4
RWT4Ca_Reg1
RWT4Ca_Reg2
RWT4Ca_+C-Tail
D
pGBKT7
pGADT7
DDO (SD-2)
QDO (SD-4)
RWT4Ca
RWT4Ca_Reg1
RWT4Ca_+C-Tail
E
K327
K217
KD
PKD
C-tail
V123R124
AvrPWT4
P
Defense gene activation
Resistance

766

767 **Figure 4. Structure-guided identification of RWT4 specificity. (A)** AlphaFold Multimer modeling
768 predicts that AvrPWT4 (orange) forms an interaction complex between the RWT4 kinase domain
769 (KD, green) and pseudokinase domain (PKD, blue). A predicted binding region V123/R124 in the
770 RWT4 KD is highlighted in cyan. pLDDT indicates confidence in structure modeling and pTM and
771 ipTM indicate the confidence for interaction. The KD and PKD were separately inputted for
772 modeling, with the linker region removed. **(B)** Illustration of sequence and structure features of
773 RWT4^{Ca}. *Rwt4* sequences were obtained from resistant wheat cultivars (Norin 4, Cadenza, Jagger,
774 Paragon, and Claire) and susceptible wheat cultivars (Chinese Spring and CDC Stanley). Kinase
775 active sites K217 and K327 are indicated in red. The interaction regions were identified based on
776 the modeling from (A). **(C)** RWT4^{Ca} variants validate the requirement of Region 1 and C-terminal
777 sequences for defense activation. *Rwt4^{Ca}* and its variants (*Rwt4*^{Ca_Reg1}: V123L/R124T, *Rwt4*^{Ca_Reg2}:
778 R627T, *Rwt4*$^{Ca_+C\text{-}Tail}$: RWT4^{Ca} with the extended C-terminal residues FIQVDQ) were co-transfected
779 with *AvrPwt4* into rice protoplasts. Cell viability was measured as ATP activity presented in
780 luminance (cd/m^2). Data are represented as the mean ± SEM (n= 5). Different letters indicate
781 significant differences using one-way ANOVA with post-hoc Tukey HSD ($P \leq 0.05$). **(D)** Yeast-two
782 hybrid confirms the interaction between CaRWT4 variants to AvrPWT4. *CaRwt4* and its variants
783 *Rwt4*^{Ca_Reg1}, and *Rwt4*$^{Ca_+C\text{-}Tail}$ were cloned to the bait vector pGBKT7 while *AvrPwt4* was cloned to
784 the prey vector pGADT7. The transformation of bait and prey vectors were confirmed by yeast
785 growth on DDO (SD-Leu/-Trp) media. The interaction was assayed by growth on QDO (SD-Ade/-
786 His/-Leu/-Trp/3-amino-1,2,4-triazole) media. Serial dilutions from cell suspensions of a single
787 yeast colony expressing the bait and prey plasmids are shown and represent the strength of
788 interaction. Empty vectors (EV) of pGBKT7 and pGADT7 were used as negative controls. **(E)** RWT4
789 working model. KD: kinase domain. PKD: Pseudokinase domain. P: phosphorylation. K217 and
790 K327: RWT4^{Ca} kinase active sites. V123/R124: AvrPWT4 binding site. C-tail: C-terminus tail of
791 RWT4. Dash: RWT4-AvrPWT4 interaction. Figure created with BioRender.com.
792
793
794
795